Check for updates
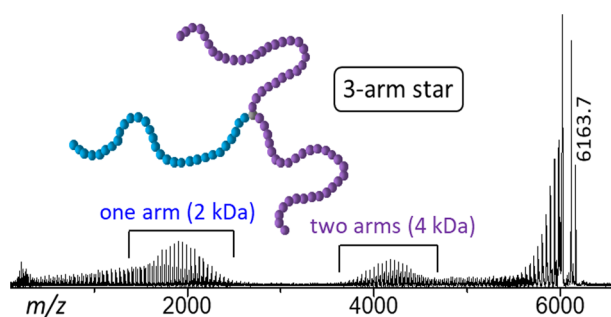
Elucidating Branching Topology and Branch Lengths in Star-Branched Polymers by Tandem Mass Spectrometry

Jialin Mao,[1] Boyu Zhang,[2] Hong Zhang,[2] Ravinder Elupula,[2] Scott M. Grayson,[2] Chrys Wesdemiotis[1]

[1]Department of Chemistry, Knight Chemical Laboratory, The University of Akron, Akron, OH 44325-3601, USA
[2]Department of Chemistry, Tulane University, New Orleans, LA 70118, USA

Abstract. Tandem mass spectrometry (MS^2) has been employed to elucidate the topology and branching architecture of star-branched polyethers. The polymers were ionized by matrix-assisted laser desorption/ionization (MALDI) to positive ions and dissociated after leaving the ion source via laser-induced fragmentation. The bond scissions caused under MALDI-MS^2 conditions occur preferentially near the core-branch joining points due to energetically favorable homolytic and heterolytic bond cleavages near the core and release of steric strain and/or reduction of crowding. This unique fragmentation mode detaches complete arms from the core generating fragment ion series at the expected molecular weight of each branch. The number of fragment ion distributions observed combined with their mass-to-charge ratios permit conclusive determination of the degree of branching and the corresponding branch lengths, as demonstrated for differently branched homo- and mikto-arm polyether stars synthesized via azide-alkyne click chemistry. The results of this study underscore the utility of MS^2 for the characterization of branching architecture and branch lengths of (co) polymers with two or more linear chains attached to a functionalized central core.

Keywords: Star-branched polymers, Tandem mass spectrometry, Polymer architecture, Degree of branching, Branch lengths

Introduction

Star polymers are branched macromolecules consisting of several linear polymeric chains radiating from a relatively small central core [1–3]. The distinctive topology of star polymers provides multiple functional groups and leads to lower hydrodynamic volume, lower viscosity, and lower degree of aggregation in solution as compared to linear polymers with similar molecular weight [1, 4–7]. The unique chemical and physical properties resulting from such features make star polymers particularly suitable for a variety of applications, including catalysis [8], imaging [9, 10], coatings [11], and drug/gene delivery [1, 12–16]. The properties of star-branched polymers are strongly affected by the chemical structure of the central core and each arm, degree of branching, and individual arm length [3, 4]. Consequently, characterization of the number of branches and the length of each branch is essential to develop star polymers with optimal physicochemical properties for the desired application.

Two appropriate mass spectrometry (MS) methods for the determination of architectural and topology features of synthetic polymers are tandem mass spectrometry (MS^2) [17] and ion mobility mass spectrometry (IM-MS) [17–20], which reveal microstructure detail by probing the fragmentation chemistry

or size/shape of the analyzed sample, respectively. IM-MS studies on branched polyethers [21] and glycopolymers [22] have documented that multiple charging (≥ 2) is needed to cause visible differences in the 3-D sizes/shapes of the branched polymer vs. a linear polymer with similar molecular weight. This prerequisite restricts the use of IM-MS to polymers that can be ionized by electrospray ionization (ESI) and are large enough to support

multiple charges. For smaller oligomers and prepolymers (M_n < 8000 Da), MS^2 could be more suitable as this method can provide sequence and connectivity insight for singly charged sample ions [17, 23].

MS^2 experiments via collisionally activated dissociation (CAD) or laser-induced fragmentation (LIFT) [24] have been performed in positive ion mode on polymers with linear [25–31], cyclic [32–37], branched [22, 38], and dendritic [39]
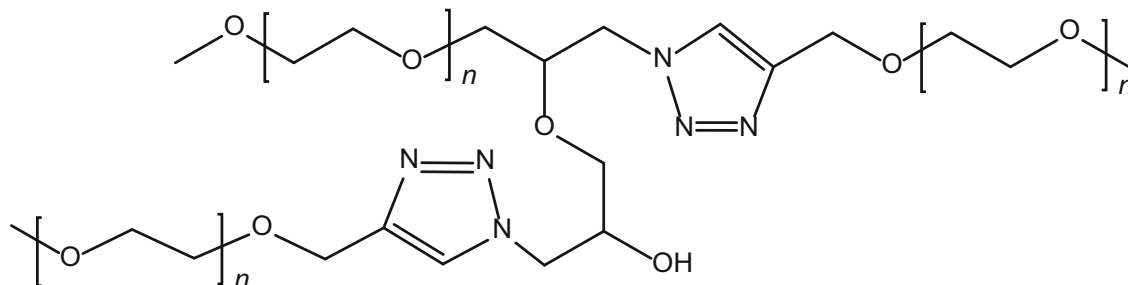
(a) 2-arm mikto-star with 2 kDa and 750 Da PEG arms
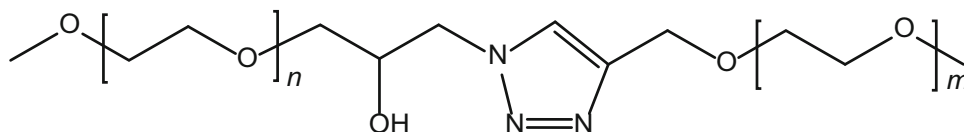
(b) 2-arm homo-star with 2 kDa PEG arms
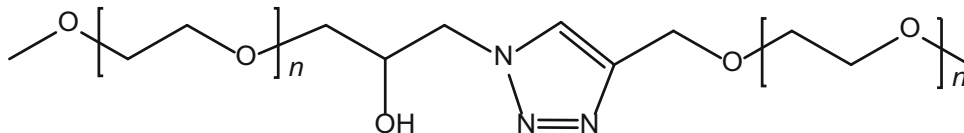
(c) 3-arm homo-star with 2 kDa PEG arms

(d) linear MeO-PEG-OMe
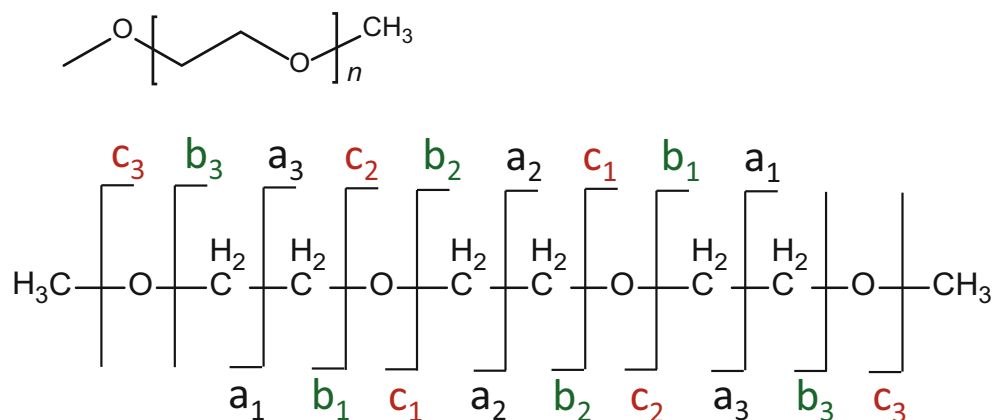
Figure 1. Structures of (**a**) 2-arm mikto-star (2-kDa and 750-Da PEG arms), (**b**) 2-arm homo-star (2-kDa PEG arms), and (**c**) 3-arm homo-star (2-kDa arms) investigated. (**d**) Nomenclature scheme for the fragments from a linear PEG with methoxy end groups, which is also applied to the star-branched PEG polymers (all contain methoxy chain ends). The bond cleavages create a new end group which is usually a carbonyl (for c_n) or vinyl functionality (for b_n); see also text

architectures to identify their primary structures. Previous MS^2 studies on branched polymers aimed at proving the presence of branched architecture(s) by detecting fragments that were impossible to form by isomeric linear structures [22, 38]. The present work investigates for the first time whether MS^2 can be employed to ascertain specific, important structural features of star-branched polyethers, namely their number of branches and the corresponding branch lengths. The polymers were ionized by matrix-assisted laser desorption ionization (MALDI) which is widely employed in polymer laboratories and typically generates singly charged ions. As will be shown in this study, arms emanating from a central, functionalized core are readily cleaved under MALDI-MS^2 conditions, thus revealing the number of branches and the individual arm chain lengths.

Experimental

Mass Spectrometry

MALDI-MS and MALDI-MS^2 spectra were measured on a Bruker UltraFlex-III MALDI-ToF/ToF mass spectrometer (Bruker Daltonics, Billerica, MA) equipped with a Nd: YAG laser (355 nm). Solutions of the matrix, trans-2-[3-(4-tert-butylphenyl)-2-methyl-2-propenylidene] malononitrile (DCTB, Alfa Aesar, 99 + %), sodium trifluoroacetate cationizing salt (NaTFA, Aldrich, 98%), and the star polymers were prepared in tetrahydrofuran (THF, Aldrich, 99.9%) at concentrations of 20 mg/mL, 10 mg/mL, and 10 mg/mL, respectively. Matrix and salt were mixed in the ratio 10:1 (v/v). About 0.5 μL of matrix/salt mixture was deposited onto a sample spot of the 384-well ground steel target plate and
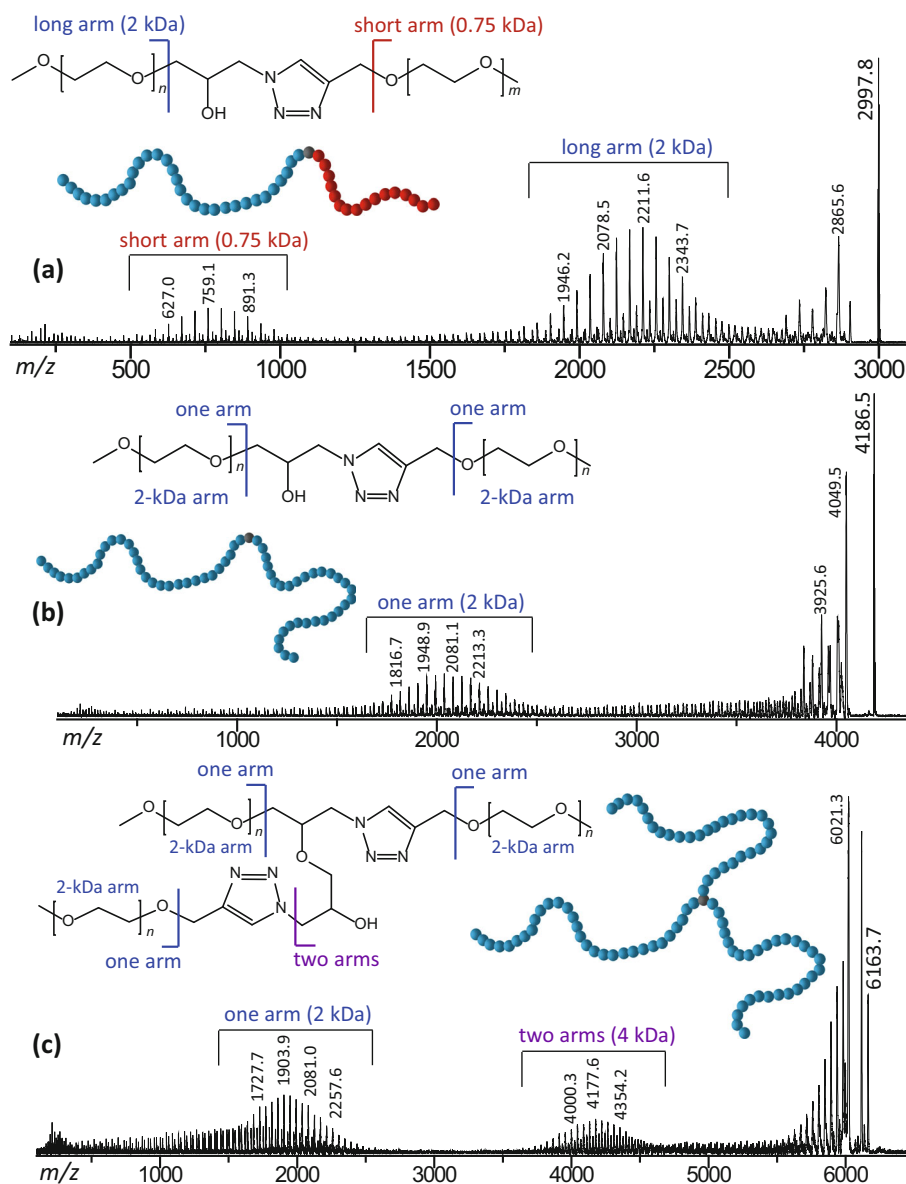
Figure 2. MALDI-MS^2 spectra of the [M + Na]$^+$ ions from the (**a**) 63-mer of the 2-arm mikto-star (*m/z* 2997.8), (**b**) 90-mer of the 2-arm homo-star (*m/z* 4186.5), and (**c**) 131-mer of the 3-arm homo-star (*m/z* 6163.7); *m/z* values are labeled on top of select ions

allowed to dry under ambient conditions. About 0.5 μL of the star polymer solution was then deposited on top of the dried matrix/salt, followed by another 0.5 μL of matrix/salt mixture onto the dried polymer. The sample spots were completely dry before the target plate was introduced into the mass spectrometer. This three-layer sandwich sample preparation protocol led to the formation of abundant $[M + Na]^+$ ions from the star polymers. The mass-to-charge ratio (m/z) scale was calibrated by poly(methyl methacrylate) (PMMA) standards with a molecular weight close to the expected mass of the samples.

The ToF/ToF instrument used consists of a short linear ToF analyzer coupled to a reflectron ToF tube; this configuration permits both MALDI-MS as well as MALDI-MS^2 analyses. For single-stage MALDI-MS spectra, both ToF devices are used as a single-reflectron ToF mass spectrometer. MALDI-MS^2 spectra are acquired using the LIFT mode [24, 40]. It involves the use of (1) increased laser intensity to activate the precursor ions so that they undergo post-source decay (PSD) in the linear ToF region; (2) isolation of the desired precursor ion and its fragments,

which move with the same velocity, by a timed ion selector (TIS); and (3) post-acceleration of the isolated ions for mass analysis in the reflectron ToF region [24, 40].

ESI-MS^2 experiments were performed on a Waters Synapt quadrupole/time-of-flight (Q/ToF) mass spectrometer (Waters, Milford, MA) at the settings described in the supporting information. Solutions of the star polymers in THF (0.1 mg/mL) were directly injected into the ESI source with a syringe pump at a flow rate of 10 μL/min. Precursor ions were mass-selected by Q and induced to fragment via collisionally activated dissociation (CAD) in the trap cell located between the Q and ToF analyzers.

Polymers

A set of high purity homo-arm and mikto-arm poly(ethylene glycol) (PEG) star polymers were synthesized by a stepwise "graft onto" method [4, 41] utilizing epoxide ring-opening and copper-catalyzed azide-alkyne cycloaddition (CuAAC) "click" chemistry [42] to attach monomethoxy-terminated linear PEG chains with an average molecular weight (M_n) of 2 kDa or 750 Da (Sigma-Aldrich, St. Louis, MO) to the same core. The
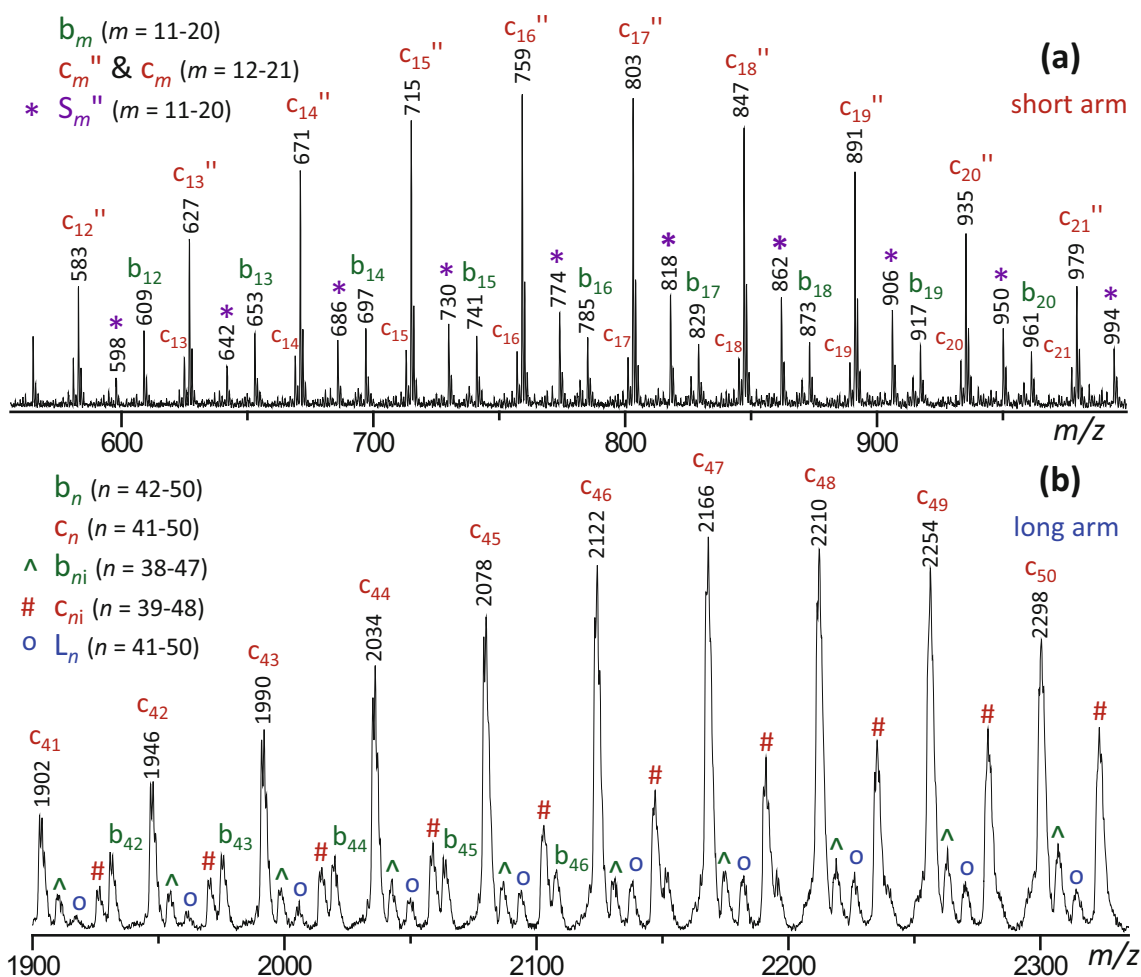
Figure 3. Expanded views of the (**a**) lower and (**b**) higher mass regions in the MALDI-MS^2 spectrum of the sodiated 63-mer of the 2-arm mikto-star (m/z 2997.8), showing the fragments containing the (**a**) short and (**b**) long PEG arm, respectively; m/z values are labeled on top of select peaks. See text and Schemes 1, 2, 3, and 4 and S1-S2 for the structures and nomenclature of the fragment series observed; a subscripted letter (i) indicates the inclusion of the internal linking substituent

PEG star polymers prepared by this approach are shown in Figure 1 and include a 2-arm mikto-star (2-kDa and 750-Da PEG chains), a 2-arm homo-star (2-kDa PEG chains), and a 3-arm homo-star (2-kDa PEG chains). The step-by-step synthesis of such architectures has been reported in a previous publication [43]. The raw synthetic products were purified by vacuum filtration, precipitation in cold hexane, and further purification by size exclusion chromatography on a Bio-Beads resin (Bio-Rad Laboratories, Hercules, CA) [43].

Results and Discussion

The MALDI-MS spectra of the star-branched polymers show single and narrow molecular weight distributions in the expected molecular weight ranges (cf. Fig. S1). The m/z values of the observed oligomers in each spectrum correspond to $[M + Na]^+$ ions with the desired core functionality and methyl groups at all chain ends [43]. MALDI-MS confirms the exceptional purity and composition of the star polymers but provides no insight on their architectures.

The MALDI-MS^2 spectra of select oligomers near the average molecular weight of the 2-arm mikto-star (2- and 0.75-kDa PEG arms), 2-arm homo-star (2-kDa PEG arms), and 3-arm homo-star (2-kDa PEG arms) are depicted in Figure 2; all were acquired in positive ion mode using the LIFT technique. Two major fragment distributions are observed for the 2-arm mikto-star (Figure 2a), one centered at $m/z \sim 750$ and the other at $m/z \sim 2000$. This result is in excellent agreement with the proposed structure which was synthesized using one short (750 Da) and one long (2 kDa) PEG arm. Conversely, the 2-arm homo-star prepared from 2-kDa PEG arms gives rise to only one major fragment distribution, centered at $m/z \sim 2000$ (Figure 2b), consistent with having two equally sized arms in this case. Meanwhile, two major fragment distributions are observed for the 3-arm homo-star with 2-kDa arms, one centered at $m/z \sim 2000$ and the other at $m/z \sim 4000$, corresponding to fragments that contain one arm and two arms, respectively. The MALDI-MS^2 data of Figure 2 indicate that bond cleavages occur preferentially at the core-branch joining points. The released arms are observed at the molecular weights of the original polymer chain reactants, thus allowing for the determination of the identity and length of the arms. Furthermore, the number of fragment distributions, combined with their average masses, reveals the number of arms and degree of branching. Fairly similar fragmentation patterns are obtained by ESI-MS^2 (cf. Fig. S2). It is worth noting, however, that ESI produces molecular ions in many different charge states and that ESI-MS^2 experiments on the doubly or more highly charged precursor ions generates fragment distributions varying in mass and charge, thus making spectral analysis and architectural assignments more challenging. In contrast, MALDI-MS^2 leads to spectra with markedly less complexity that are easier to interpret.

Bond cleavages at or near the core-branch joining points could be favored for several reasons. The release of steric strain and the reduction of crowding near the core could contribute to the preference of such dissociations, especially for the more highly branched architecture. The main cause of such reactivity is presumably the stabilization provided by the core to the ionic or radical intermediates traversed during fragmentation. Indeed, all major fragment series formed upon MS^2 are
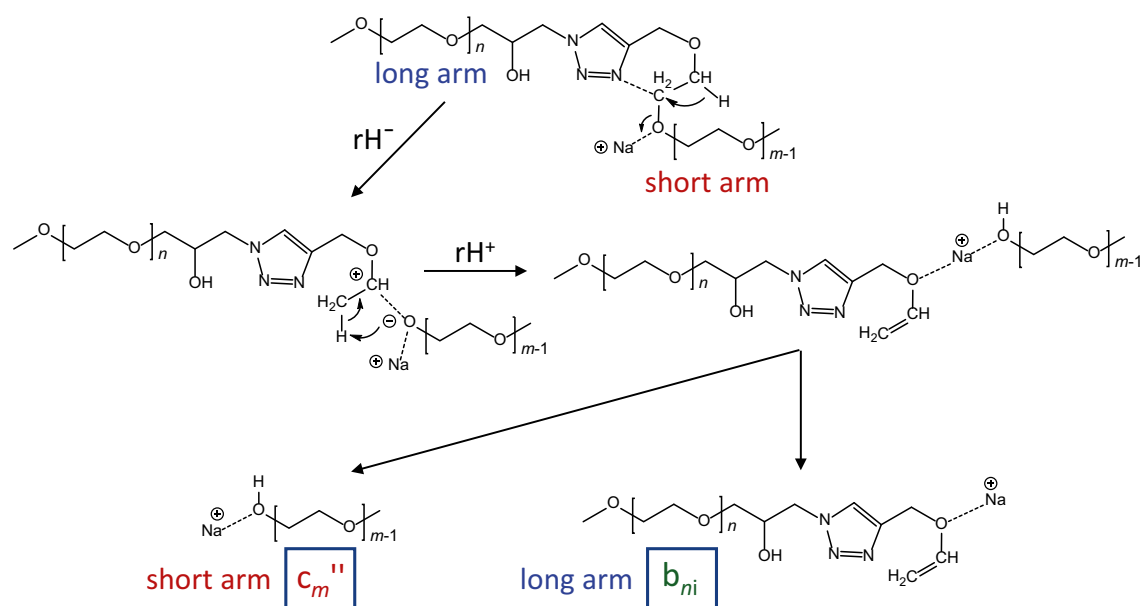
Scheme 1. Charge-induced dissociation of a C–O bond in the short arm of the sodiated 2-arm mikto-star (2-kDa and 0.75-kDa PEG arms), generating fragments with (b$_{ni}$) or without (c$_m''$) the linking substituent; rH$^-$ and rH$^+$ designate hydride and proton transfer, respectively. The n and m subscripts refer to fragments containing the long PEG chain or short PEG chain, respectively. The subscripted letter ($_i$) denotes the inclusion of the internal linker and the superscripted double prime symbol ($''$) denotes a newly formed saturated chain end (the hydroxy group of c$_m''$)

reconciled by charge-induced or charge-remote dissociations at or near the triazole ring, as discussed for the three stars examined in the following sections.

2-Arm Mikto-Star (2-kDa and 750-Da PEG Arms)

Metal-cationized polyether ions generally dissociate via both charge-induced as well as charge-remote reactions that cleave the ether bonds [23, 44]. The predominant fragmentation mode is determined by the size of the dissociating ion and the degree of activation. Earlier studies have indicated that short PEG chains dissociate by either mechanism, with charge-induced dissociations favored at low internal energies (and vice versa), whereas longer PEGs (~ 2000 Da and beyond) largely fragment through charge-remote processes [23, 45]. Both types of these chains are present in the 2-arm mikto-star. Further, either of the two carbon-oxygen bonds in the C–O–C ether functionality can be cleaved, and each one may lead to different fragments for asymmetrically substituted PEG chains like the 2-arm mikto-star; for differentiation, these two types of bond cleavages will be referred to as C–O and O–C bond dissociation. Both of these dissociations generate two products: one including the short chain (m repeat units) and the other the long chain (n repeat units); one of these products will also contain the internal linking substituent (indicated by a subscripted letter ($_i$)). Note that all fragments contain one CH_3O- chain end from the PEG reactants used to synthesize the stars. Fragmentation creates a new chain end (cf. series b_n and c_n in Figure 1); these newly created chain ends can be unsaturated (b_n or c_n) or saturated in which case they are designated with a double prime (for example, c_n'').

Charge-induced dissociation near the core-branch juncture of the short arm accounts for two of the homologous fragment series observed, viz. c_m'' from the short arm (Figure 3a) and b_{ni}'' from the long arm (Figure 3b). Scheme 1 presents a mechanistic rationalization for this reaction pathway, which is promoted by the Lewis acid character of the Na^+ charge. Na^+ coordination at the O atom of a C–O bond weakens this bond, facilitating heterolytic cleavage. An unstable primary carbocation and a sodium alkoxylate emerge from this bond cleavage, which can rearrange via an energetically favorable 1,2-hydride transfer to a more stable ion-dipole complex between a secondary alkoxyethyl cation and a sodium alkoxylate. Proton transfer from the carbocation to the negatively charged alkoxylate, accompanied by Na^+ ligand rearrangement, produces a Na^+-bound complex of the separated chain segments, which can
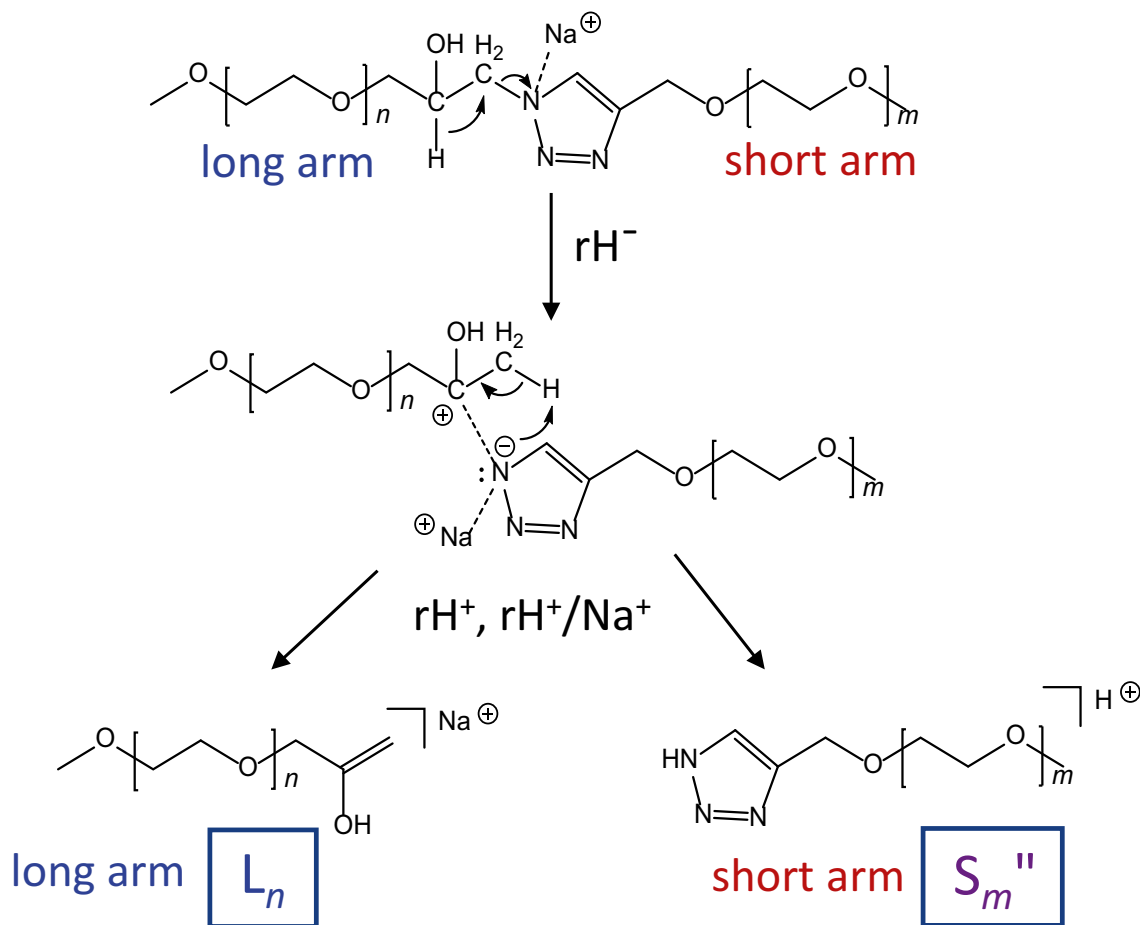

Scheme 2. Charge-induced dissociation of the C–N bond in the long arm of the sodiated 2-arm mikto-star (2-kDa and 0.75-kDa PEG arms), generating fragments that contain parts of the linking substituent and either the long (L_n) or short (S_m'') PEG chain; rH^-, rH^+, and rH^+/Na^+ designate hydride transfer, proton transfer, and H^+/Na^+ exchange, respectively

dissociate to yield fragment c_m'' (short chain with saturated chain end) or b_{ni} (long chain with linker and vinyl chain end). In a linear unsubstituted PEG, such C–O bond scission can take place anywhere along the chain [23, 45]. In the triazole functionalized 2-arm mikto-star, this dissociation occurs preferably on the short arm next to the triazole linker, where the nascent primary carbocation emerging after C–O bond dissociation can be stabilized by electrostatic interaction (intramolecular solvation) with a basic triazole nitrogen atom, as shown in Scheme 1 (note that the hydroxy group on the long arm is most likely hydrogen-bonded to the nearby triazole nitrogen atom, thereby obstructing a similar neighboring group effect in the long arm).

The unique substitution pattern at the long arm of the mikto-star enables a different charge-induced fragmentation mode that detaches the entire long arm at the triazole junction to create fragment series S_m'' (Figure 3a) and L_n (Figure 3b) comprising the complete short arm or long arm, respectively (cf. Scheme 2). Here, heterolytic C–N bond cleavage catalyzed by the Na$^+$ Lewis acid and concomitant 1,2-hydride shift produce a tertiary carbocation interacting with an amide anion. Proton abstraction from the carbocation by the amide nitrogen and H$^+$/Na$^+$ exchange between the detaching segments gives rise to the mentioned fragment ions. The oxygen-rich long arm is detected in sodiated form, whereas the nitrogen-rich (more basic) short arm is observed protonated. The newly formed end groups of homologous series S_m'' and L_n confirm the core-branch connectivity of the 2-arm mikto-star.

The reactions discussed compete with charge-remote fragmentations [46], which are most prevalent in longer polyether chains, where the metal ion is well sequestered by several ether oxygens and cannot easily be mobilized to the reactive site to induce heterolytic bond cleavage. Several of the observed fragment series are reconciled by charge-remote homolytic ether bond cleavages which, again, are preferred near the core-branch junction where newly formed radicals can be stabilized by the adjacent triazole ring. Scheme 3a illustrates such a pathway for the O–C bond nearest to the triazole junction on the long arm. Homolytic scission of this bond creates two incipient radical ions, viz. $c_n^\bullet$ and $b_{mi}^\bullet$. Consecutive H$^\bullet$ loss from $c_n^\bullet$ gives rise to series c_n comprising the long arm and an aldehyde end group (dominant fragments in Figure 3b). Interestingly, the complementary series, b_{mi}, formed by H$^\bullet$ loss from, $b_{mi}^\bullet$, is not observed; this is attributed to the proximity of the triazole ring, which enables rearrangement of the incipient $b_{mi}^\bullet$ radical ions to more stable isomeric species that expel the linker to yield $c_m^\bullet$ and, by consecutive H$^\bullet$ loss, series c_m comprising the short arm and an aldehyde end group and appearing 2 m/z units below series c_m'' (Figure 3a). A similar charge-remote pathway initiated by cleavage of the C-O bond nearest to the triazole junction on the long arm (Schemes 3b and S1) leads to fragment series b_n and c_m (Figures 3b and 3a, respectively).

Charge-remote homolytic ether bond cleavages also take place in the short arm (Schemes 4 and S2). Once more,
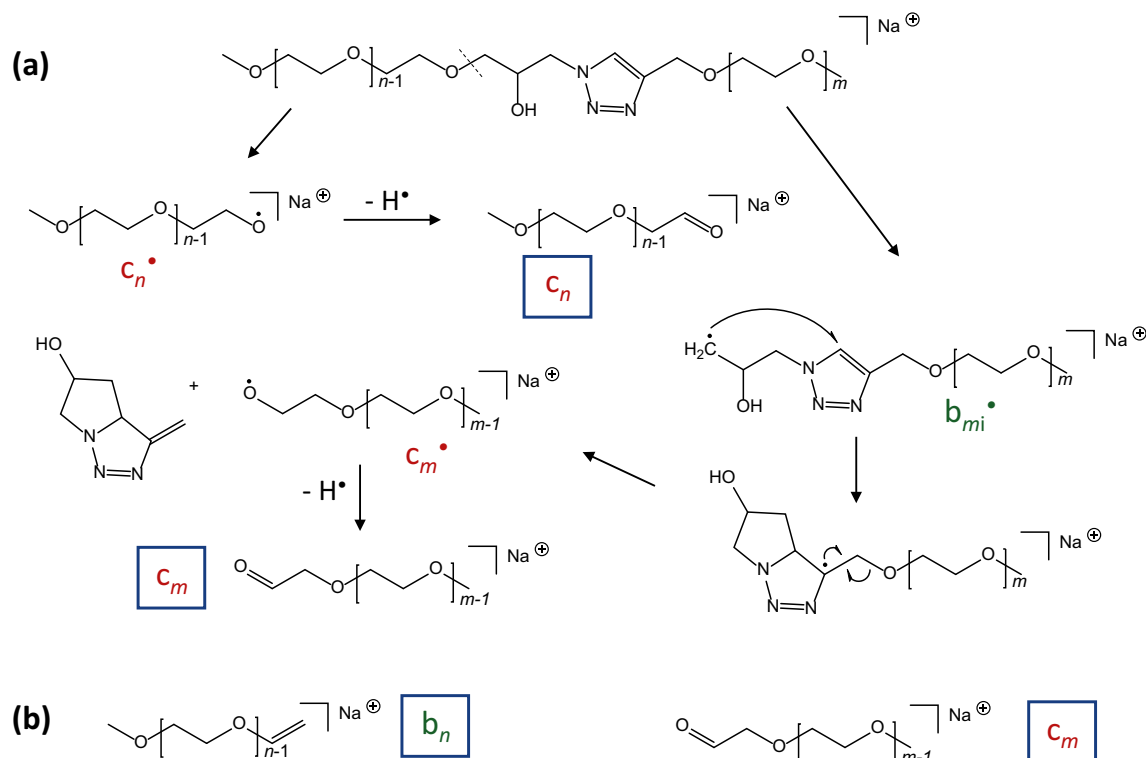
Scheme 3. Charge-remote homolytic (**a**) O–C and (**b**) C–O bond dissociation in the long arm of the 2-arm mikto-star (2-kDa and 0.75-kDa PEG chains), generating fragments with a terminal double bond and containing either the long arm (c_n and b_n) or the short arm (c_m). See Scheme S1 for the detailed pathway to the b_n + c_m fragments originating via a similar mechanism from C–O bond dissociation
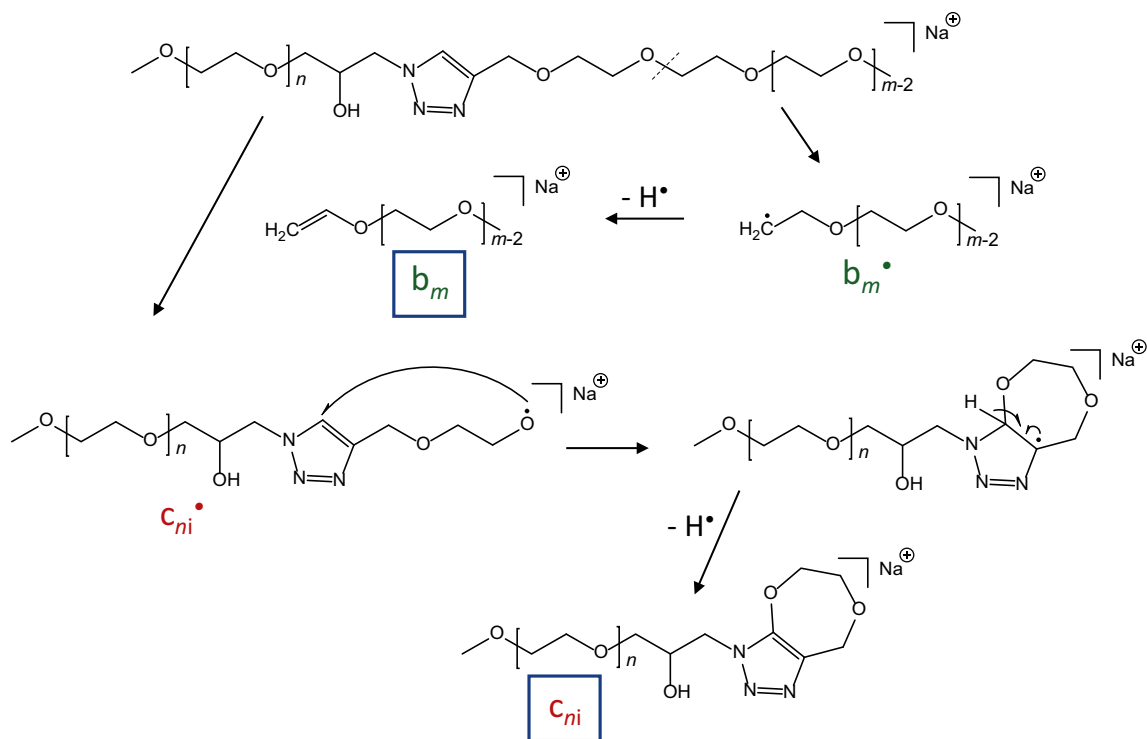
Scheme 4. Charge-remote homolytic O–C bond dissociation in the short arm of the 2-arm mikto-star (2-kDa and 0.75-kDa PEG chains), generating fragments with a double bond in their chain ends and containing either the short arm (b_m) or the long arm plus the linker as end group (c_{ni})

dissociation of bonds proximate to the core-branch junction is favored due to the stabilization the triazole ring can provide to one of the radicals arising upon ether bond scission. Because of the different substitution pattern on the short arm side, the rearranged radical ions do not expel the linker in this case, but rather lose an H• radical to form a double bond at the newly created end group. The overall reaction sequence commences with homolysis of the O–C or C–O bond near the triazole ring and ultimately gives rise to fragment series $b_m + c_{ni}$ (Scheme 4) or fragment series $c_m + b_{ni}$ (Scheme S2), respectively.

It is worth noting that the MALDI-MS^2 spectrum of the 2-arm mikto-star (Figure 2a) is dramatically different from the
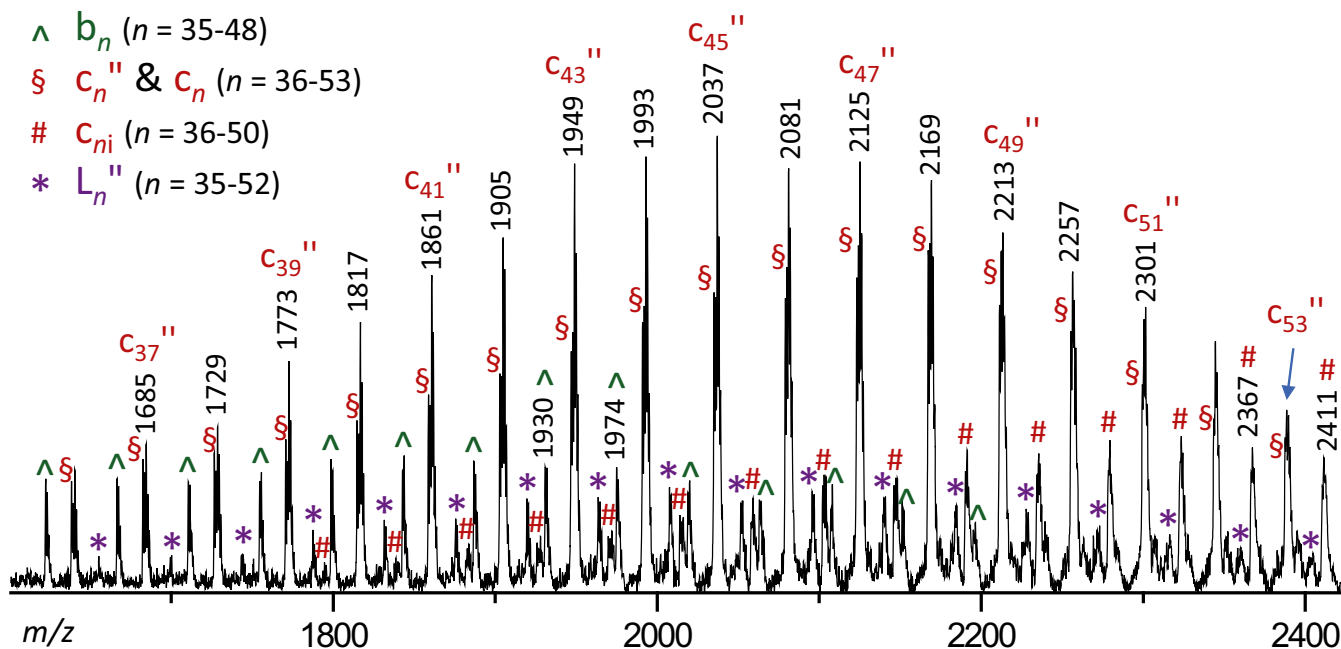
Figure 4. Expanded view of the m/z 1600–2400 region in the MALDI-MS^2 spectrum of the sodiated 90-mer of the 2-arm homo-star (m/z 4186.5), showing the dominant fragment distributions containing one PEG arm; m/z values are labeled on top of select peaks

MALDI-MS^2 spectra reported for linear PEG architectures, which show fragments from random ether bond cleavages across the entire chain and stretching from the molecular ion region down to $m/z < 200$ [23]. For comparative purpose, the MALDI-MS^2 spectrum of the sodiated 47-mer from linear CH$_3$O–PEG–OH (m/z 2124.3) is shown in Fig. S3. Linear PEGs and star-branched congeners with a triazole core can readily be differentiated based on the distinct fragmentation patterns in Figure 2a vs. Fig. S3.
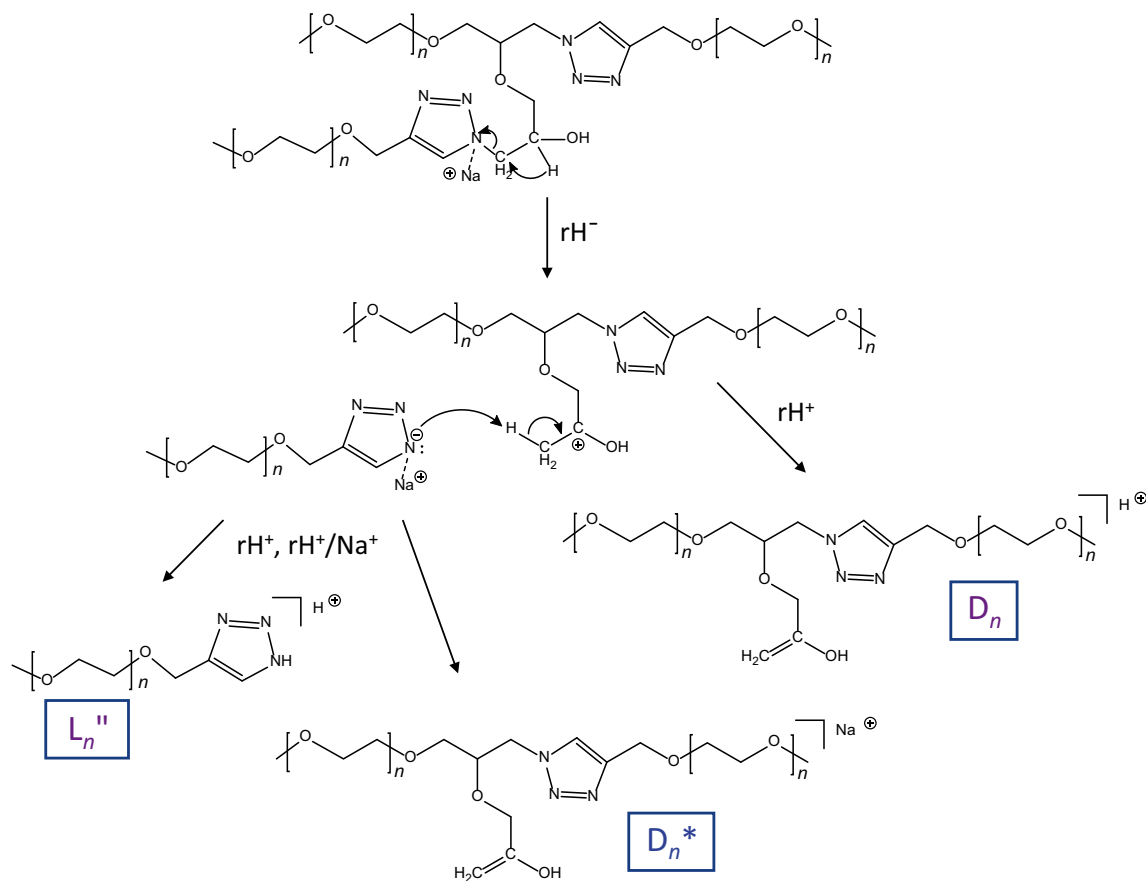
2-Arm Homo-Star (2-kDa PEG Arms)

The 2-arm homo-star generates only one major distribution upon MALDI-MS^2 (cf. Figures 2b and 4), as the two PEG arms of this polymer have the same size. The two arms are, however, linked differently to the triazole core: one is attached to a triazole carbon atom, similar to the short arm of the mikto-star, while the other is connected to a triazole nitrogen atom through a hydroxy-substituted bridge, like the long arm of the mikto-star. As a consequence, the homo-star undergoes the same types of dissociations encountered with the corresponding mikto-star, including charge-induced fragmentation via the pathways of Scheme 1 (to c_n'') and Scheme 2 (to L_n'' (the same connectivity as S_m'' in Scheme 2) as well as charge-remote

fragmentation via the pathways of Scheme 3 (to $c_n + b_n$) and Scheme 4 (to $b_n + c_{ni}$), cf. Figure 4.

3-Arm Homo-Star (2-kDa PEG Arms)

Two major fragment distributions are present in the MALDI-MS^2 spectrum of the 3-arm homo-star, centered at around m/z 2000 and 4000 and arising from fragment ions with one and two 2-kDa PEG arms, respectively. The fragments in the $m/z \sim 2000$ region include (in decreasing relative intensity) series c_n'', c_n, b_n, and L_n'' (Fig. S4a); this fragmentation pattern is similar with that obtained from the 2-arm homo-star (Figure 4). The dominant series in the $m/z \sim 4000$ region (Fig. S4b) contain the 2-arm fragment D_n/D_n^* which is co-produced with L_n'' by charge-induced N–C bond cleavage, as rationalized in Scheme 5. This fragment is observed both in the protonated form (D_n), due to the inclusion of a basic triazole moiety, as well as in sodiated form (D_n^*), due to the presence of two long polyether chains. The reduction of crowding brought upon losing one arm must contribute to the high yield of fragments D_n/D_n^*. It is noteworthy that the 3-arm homo-star dissociates efficiently upon MALDI-MS^2 in spite of its high mass [47].

Scheme 5. Charge-induced dissociation of the N–C bond in the long arm closest to the hydroxy substituent of the sodiated 3-arm homo-star (2-kDa arms), generating fragments that contain one (L_n'') or two (D_n and D_n^*) long PEG chains; rH$^-$, rH$^+$, and rH$^+$/Na$^+$ designate hydride transfer, proton transfer, and H$^+$/Na$^+$ exchange, respectively

Conclusions

This study documented the utility of tandem mass spectrometry for the topological and architectural differentiation and characterization of star-branched polyethers synthesized using alkyne-azide click chemistry, which creates triazole linkages. The polyethers investigated encompass 2-arm mikto, 2-arm homo-, and 3-arm homo-architectures. Single-stage MALDI-MS confirmed the high purity and narrow molecular weight distribution of the analyzed samples. MALDI-MS^2 experiments further demonstrated that activation of the sodiated star polymers preferentially causes bond scissions near the triazole core-branch joining points due mainly to energetically favorable heterolytic and homolytic bond cleavages near the triazole ring and, to some extent, to release of steric strain and/or reduction of crowding as well. These factors result in the detachment of complete arms from the core to generate fragment ions at the expected molecular weight of each arm. The number of fragment distributions observed combined with the m/z values of the fragment ions permit conclusive assignment of the degree of branching and branch lengths. Analogous findings have been reported for polystyrene-based stars with arms emanating from a Si-containing core which can stabilize radical intermediates [17, 48]. The corroborating results of our study allow to project that MS^2 will be a generally useful means to determine star architecture if the arms are attached to a functional core that can stabilize ionic or radical intermediates.

Acknowledgements

References

1. Daoud, M., Cotton, J.P.: Star shaped polymers: a model for the conformation and its concentration dependence. J. Phys.-Paris. **43**, 531–538 (1982)
2. Inoue, K.: Functional dendrimers, hyperbranched and star polymers. Prog. Polym. Sci. **25**, 453–571 (2000)
3. Ren, J.M., McKenzie, T.G., Fu, Q., Wong, E.H.H., Xu, J., An, Z., Shanmugam, S., Davis, T.P., Boyer, C., Qiao, G.G.: Star polymers. Chem. Rev. **116**, 6743–6836 (2016)
4. Lapienis, G.: Star-shaped polymers having PEO arms. Prog. Polym. Sci. **34**, 852–892 (2009)
5. Khanna, K., Varshney, S., Kakkar, A.: Miktoarm star polymers: advances in synthesis, self-assembly, and applications. Polym. Chem. **1**, 1171–1185 (2010)
6. Hadjichristidis, N., Pitsikalis, M., Iatrou, H., Driva, P., Sakellariou, G., Chatzichristidi, M.: Polymers with star-related structures: synthesis, properties, and applications. In: Matyjaszewski, K., Möller, M. (eds.) Polymer science: a comprehensive reference, vol. 6, pp. 29–111. Elsevier, Amsterdam (2012)
7. Chremos, A., Jeong, C., Douglas, J.F.: Influence of polymer architectures on diffusion in unentangled polymer melts. Soft Matter. **13**, 5778–5784 (2017)
8. Rodionov, V., Gao, H., Scroggins, S., Unruh, D.A., Avestro, A.-J., Fréchet, J.M.J.: Easy access to a family of polymer catalysts from modular star polymers. J. Am. Chem. Soc. **132**, 2570–2572 (2010)
9. Li, Y., Beija, M., Laurent, S., Elst, L.V., Muller, R.N., Duong, H.T.T., Lowe, A.B., Davis, T.P., Boyer, C.: Macromolecular ligands for gadolinium MRI contrast agents. Macromolecules. **45**, 4196–4204 (2012)
10. Adkins, C.T., Dobish, J.N., Brown, C.S., Mayrsohn, B., Hamilton, S.K., Udoji, F., Radford, K., Yankeelov, T.E., Gore, J.C., Harth, E.: High relaxivity MRI imaging reagents from bimodal star polymers. Polym. Chem. **3**, 390–398 (2012)
11. Groll, J., Ademovic, Z., Ameringer, T., Klee, D., Moeller, M.: Comparison of coatings from reactive star shaped PEG-stat-PPG prepolymers and grafted linear PEG for biological and medical applications. Biomacromolecules. **6**, 956–962 (2005)
12. Jones, M.-C., Ranger, M., Leroux, J.-C.: pH-sensitive unimolecular polymeric micelles: synthesis of a novel drug carrier. Bioconjug. Chem. **14**, 774–781 (2003)
13. Meier, M.A.R., Schubert, U.S.: Combinatorial evaluation of the host-guest chemistry of star-shaped block copolymers. J. Comb. Chem. **7**, 356–359 (2005)
14. Thornton, P.D., Billah, S.M.R., Cameron, N.R.: Enzyme-degradable self-assembled hydrogels from polyalanine-modified poly(ethylene glycol) star polymers. Macromol. Rapid Comm. **34**, 257–262 (2013)
15. Ma, D., Liu, Z.-H., Zheng, Q.-Q., Zhou, X.-Y., Zhang, Y., Shi, Y.-F., Lin, J.-T., Xue, W.: Star-shaped polymer consisting of a porphyrin core and poly(L-lysine) dendron arms: synthesis, drug delivery, and in vitro chemo/photodynamic therapy. Macromol. Rapid Comm. **34**, 548–552 (2013)
16. Wu, W., Wang, W., Li, J.: Star polymers: advances in biomedical applications. Prog. Polym. Sci. **46**, 55–85 (2015)
17. Wesdemiotis, C.: Multidimensional mass spectrometry of synthetic polymers and advanced materials. Angew. Chem. Int. Ed. **56**, 1452–1464 (2017)
18. Wyttenbach, T., Gidden, J., Bowers, M.T.: Developments in ion mobility theory, instrumentation, and applications. In: Wilkins, C.L., Trimpin, S. (eds.) Ion mobility spectrometry-mass spectrometry, pp. 3–30. CRC Press, Boca Raton, FL (2011)
19. Trimpin, S., Clemmer, D.E., Larsen, B.S.: Snapshot, conformation, and bulk fragmentation: characterization of polymeric architectures using ESI-IMS-MS. In: Wilkins, C.L., Trimpin, S. (eds.) Ion mobility spectrometry-mass spectrometry, pp. 215–235. CRC Press, Boca Raton, FL (2011)
20. Bowers, M.T.: Ion mobility spectrometry: a personal view of its development at UCSB. Int. J. Mass Spectrom. **370**, 75–95 (2014)
21. Foley, C.D., Zhang, B., Alb, A.M., Trimpin, S., Grayson, S.M.: Use of ion mobility spectrometry-mass spectrometry to elucidate architectural dispersity within star polymers. ACS Macro Lett. **4**, 778–782 (2015)
22. Liu, X., Cool, L.R., Lin, K., Kasko, A.M., Wesdemiotis, C.: Tandem mass spectrometry and ion mobility mass spectrometry for the analysis of molecular sequence and architecture of hyperbranched glycopolymers. Analyst. **140**, 1182–1191 (2015)
23. Wesdemiotis, C., Solak, N., Polce, M.J., Dabney, D.E., Chaicharoen, K., Katzenmeyer, B.C.: Fragmentation pathways of polymer ions. Mass Spectrom. Rev. **30**, 523–559 (2011)
24. Scionti, V., Wesdemiotis, C.: Tandem mass spectrometry analysis of polymer structures and architectures. In: Barner-Kowollik, C., Gruendling, T., Falkenhagen, J., Weidner, S. (eds.) Mass spectrometry in polymer chemistry, pp. 57–84. Wiley-VCH, Weinheim (2012)
25. Polce, M.J., Ocampo, M., Quirk, R.P., Wesdemiotis, C.: Tandem mass spectrometry characteristics of silver-cationized polystyrenes: backbone degradation via free radical chemistry. Anal. Chem. **80**, 347–354 (2008)
26. Polce, M.J., Ocampo, M., Quirk, R.P., Leigh, A.M., Wesdemiotis, C.: Tandem mass spectrometry characteristics of silver-cationized polystyrenes: internal energy, size, and chain end versus backbone substituent effects. Anal. Chem. **80**, 355–362 (2008)
27. Gies, A.P., Geibel, J.F., Hercules, D.M.: MALDI-TOF/TOF CID study of poly(p-phenylene sulfide) fragmentation reactions. Macromolecules. **43**, 952–967 (2010)
28. Knop, K., Jahn, B.O., Hager, M.D., Crecelius, A., Gottschaldt, M., Schubert, U.S.: Systematic MALDI-TOF CID investigation on different substituted mPEG 2000. Macromol. Chem. Phys. **211**, 677–684 (2010)
29. Nasioudis, A., Memboeuf, A., Heeren, R.M.A., Smith, D.F., Vékey, K., Drahos, L., van den Brink, O.F.: Discrimination of polymers by using their characteristic collision energy in tandem mass spectrometry. Anal. Chem. **82**, 9350–9356 (2010)
30. Nasioudis, A., Heeren, R.M.A., van Doormalen, I., de Wijs-Rot, N., van den Brink, O.F.: Electrospray ionization tandem mass spectrometry of

ammonium cationized polyethers. J. Am. Soc. Mass Spectrom. **22**, 837–844 (2011)

31. Jeanne Dit Fouque, D., Maroto, A., Memboeuf, A.: Purification and quantification of an isomeric compound in a mixture by collisional excitation in multistage mass spectrometry experiments. Anal. Chem. **88**, 10821–10825 (2016)

32. Li, X., Chan, Y.-T., Newkome, G.R., Wesdemiotis, C.: Gradient tandem mass spectrometry interfaced with ion mobility separation for the characterization of supramolecular architectures. Anal. Chem. **83**, 1284–1290 (2011)

33. Fouquet, T., Phan, T.N.T., Charles, L.: Tandem mass spectrometry of electrosprayed polyhedral oligomeric silsesquioxane compounds with different substituents. Rapid Comm. Mass Spectrom. **26**, 765–774 (2012)

34. Yol, A.M., Dabney, D.E., Wang, S.-F., Laurent, B.A., Foster, M.D., Quirk, R.P., Grayson, S.M., Wesdemiotis, C.: Differentiation of linear and cyclic polymer architectures by MALDI tandem mass spectrometry (MALDI-MS^2). J. Am. Soc. Mass Spectrom. **24**, 74–82 (2013)

35. Yol, A.M., Wesdemiotis, C.: Multidimensional mass spectrometry methods for the structural characterization of cyclic polymers. React. Funct. Polym. **80**, 95–108 (2014)

36. Josse, T., De Winter, J., Dubois, P., Coulembier, O., Gerbaux, P., Memboeuf, A.: A tandem mass spectrometry-based method to assess the architectural purity of synthetic polymers: a case of a cyclic polylactide obtained by click chemistry. Polym. Chem. **6**, 64–69 (2015)

37. He, Q., Mao, J., Wesdemiotis, C., Quirk, R.P., Foster, M.D.: Synthesis and isomeric characterization of well-defined 8-shaped polystyrene using anionic polymerization, silicon chloride linking chemistry, and metathesis ring closure. Macromolecules. **50**, 5779–5789 (2017)

38. Chaicharoen, K., Polce, M.J., Singh, A., Pugh, C., Wesdemiotis, C.: Characterization of linear and branched polyacrylates by tandem mass spectrometry. Anal. Bioanal. Chem. **392**, 595–607 (2008)

39. Tintaru, A., Monnier, V., Bouillon, C., Giordanengo, R., Quéléver, G., Peng, L., Charles, L.: Structural characterization of poly(amino)ester

dendrimers and related impurities by electrospray tandem mass spectrometry. Rapid Comm. Mass Spectrom. **24**, 2207–2216 (2010)

40. Suckau, D., Resemann, A., Schuerenberg, M., Hufnagel, P., Franzen, J., Holle, A.: A novel MALDI LIFT-TOF/TOF mass spectrometer for proteomics. Anal. Bioanal. Chem. **376**, 952–965 (2003)

41. Li, Y., Zhang, B., Hoskins, J.N., Grayson, S.M.: Synthesis, purification, and characterization of "perfect" star polymers via "click" coupling. J. Polym. Sci. Polym. Chem. **50**, 1086–1101 (2012)

42. Kolb, H.C., Finn, M.G., Sharpless, K.B.: Click chemistry: diverse chemical function from a few good reactions. Angew. Chem. Int. Ed. **40**, 2004–2021 (2001)

43. Zhang, B., Zhang, H., Elupula, R., Alb, A.M., Grayson, S.M.: Efficient synthesis of high purity homo-arm and mikto-arm poly(ethylene glycol) stars using epoxide and azide-alkyne coupling chemistry. Macromol. Rapid Comm. **35**, 146–151 (2014)

44. Polce, M.J., Wesdemiotis, C.: Tandem mass spectrometry and polymer ion dissociation. In: Li, L. (ed.) MALDI mass spectrometry for synthetic polymer analysis, pp. 85–127. John Wiley & Sons, Inc., Hoboken, NJ (2009)

45. Solak, N.: Structural characterization and quantitative analysis by interfacing liquid chromatography and ion mobility separation with multidimensional mass spectrometry. Ph.D. Dissertation, The University of Akron (2009). https://etd.ohiolink.edu/pg_10?::NO:10:P10_ETD_SUBID:47341

46. Cheng, C., Gross, M.L.: Applications and mechanisms of charge-remote fragmentation. Mass Spectrom. Rev. **19**, 398–420 (2000)

47. Liu, Z., Schey, K.L.: Optimization of a MALDI TOF-TOF mass spectrometer for intact protein analysis. J. Am. Soc. Mass Spectrom. **16**, 482–490 (2005)

48. Yol, A.M.: Determination of polymer structures, sequences, and architectures by multidimensional mass spectrometry. Ph.D. Dissertation, The University of Akron (2013). https://etd.ohiolink.edu/pg_10?::NO:10:P10_ETD_SUBID:88724